

Magnetic anisotropy behaviour of pyrrhotite as determined by low- and high-field experiments

F. Martín-Hernández,^{1*} M. J. Dekkers,¹ I. M. A. Bominaar-Silkens² and J. C. Maan²

¹Paleomagnetic Laboratory "Fort Hoofdijk", Faculty of Geosciences, Utrecht University, The Netherlands. E-mail: fatima@fis.uem.es

²High Field Magnetic Laboratory, Institute for Molecules and Materials, Radboud University Nijmegen, The Netherlands

Accepted 2008 March 13. Received 2008 March 13; in original form 2007 March 23

SUMMARY

Here we report on the sources of magnetic anisotropy in pyrrhotite, an iron sulphide present in many rocks as an important carrier of the Natural Remanent Magnetization. While the magnetic hysteresis parameters of pyrrhotite are well known, the existing database concerning its anisotropy behaviour is patchy and ambiguous. Therefore, a collection of 11 seemingly single crystals of natural pyrrhotite was scrutinized. Before embarking on the anisotropy determinations the set of single crystals was extensively characterized rock magnetically by measuring Curie temperatures, hysteresis loops, IRM acquisition curves, and FORC diagrams (the latter three all at room temperature). First the variation of the low-field susceptibility as function of applied field and grain size was evaluated for fields ranging from 1 to 450 A m⁻¹. Existing grain size dependent data and the present larger crystals show a logarithmic grain size dependence. This enables estimating the grain size for unimodal pyrrhotite distributions in rocks. Measured trends are better fitted with an exponential function than with a Rayleigh Law style function. Based on the rock magnetic characterization and the behaviour of the anisotropy of magnetic susceptibility six samples (of the original 11) were selected for the high-field anisotropy determinations within the basal plane. Those data were acquired with a torque cantilever-type magnetometer. As expected, most single crystals showed a pure 6- θ curve within their basal plane because of the easy axis configuration. In some crystals, however, lower harmonic terms overlapped the 6- θ term. This may be the dominant source of the observed variation in magnetic anisotropy properties. Torque data of three of the six samples were of sufficient quality to allow evaluation of K_1 . Re-evaluation of existing torque data and including the present newly derived determinations, yields for the anisotropy constant of pyrrhotite within the basal plane K_1 : $(2.7 \pm 0.2) 10^4 \text{ Jm}^{-3}$. This is over an order of magnitude more precise than the sparse existing K_1 data; only the value reported by Mikami and co-authors in 1959 agrees with the new determination. With this firmly established K_1 value meaningful anisotropy models are now possible for pyrrhotite-bearing rocks.

Keywords: Magnetic and electrical properties; Magnetic fabrics and anisotropy; Magnetic mineralogy and petrology; Rock and mineral magnetism.

1 INTRODUCTION

Pyrrhotite is an iron sulphide solid solution series with compositions in the range Fe₇S₈–Fe₁₁S₁₂. It occurs in trace amounts in many rock types: it has been reported in igneous, metamorphic, sedimentary rocks, and also in meteorites (e.g. Snowball & Torii 1999; Evans & Heller 2003). The pyrrhotite crystal structure is based on the hexagonal NiAs structure (e.g. Dunlop & Özdemir 1997). Indeed most pyrrhotite compositions (Fe₉S₁₀–Fe₁₁S₁₂) are hexagonal and only the most iron-deficient composition (Fe₇S₈) has a monoclinic

structure which however can still be considered pseudo-hexagonal (monoclinic β angle is 90.4 °) (Bennett & Graham 1980; Bennett & Graham 1981). The stacking of Fe in the S interstices along the hexagonal c -axis gives rise to various superstructures (often labelled NC after Morimoto *et al.* (1970) with N between 4 and 6) depending on the overall pyrrhotite composition. In monoclinic 4C pyrrhotite the Fe vacancies occur each other layer (Bertaut 1953) giving rise to ferrimagnetism. All other pyrrhotite compositions are antiferromagnetic at room temperature (Schwarz & Vaughan 1972; Vaughan & Graig 1978; Bennett & Graham 1980; Bennett & Graham 1981). They become ferrimagnetic around 200 °C with a superstructure often labelled NA that is subtly different from the NC structures. The transition temperature depends on the pyrrhotite composition and gives rise to a λ shaped peak in magnetization versus temperature

*Now at the Department of Geophysics, Faculty of Physics, Universidad Complutense de Madrid, Spain.

curves. Therefore, this transition is referred to as λ or γ transition (e.g. Schwarz & Vaughan 1972). In pyrrhotite-bearing ores often various superstructures are intergrown (e.g. Arnold 1967; Naldrett & Kullerud 1967; Schwarz & Vaughan 1972; Zapletal 1993) giving rise to mixed magnetic properties.

1.1 Magnetocrystalline anisotropy constant of pyrrhotite

Magnetically, pyrrhotite is extremely anisotropic with magnetite-like low-field susceptibility values within the basal plane and values typical of antiferromagnetic material along the crystallographic c -axis perpendicular to the basal plane (Schwarz 1975). Because of its overall hexagonal structure a triaxial anisotropy occurs within the basal plane. Mikami *et al.* (1959) proposed a model to explain this magnetic anisotropy, based on the lattice potential energy computed by Bertaut (1953). The model suggests the presence of three small crystal domains with pseudo-orthorhombic symmetry; each domain has a common c -axis and their a - and b -axis are distributed in the basal plane with an angle of 60° . The literature database of reported K_1 values consists of four studies only, two of them derived K_1 from high-field torque magnetometry (Mikami *et al.* 1959; Hirone *et al.* 1962) and the other two deduced K_1 from the analysis of magnetization curves (Bin & Pauthenet 1963; Sato *et al.* 1964). The corresponding magnetocrystalline anisotropy constant K_1 is rather poorly constrained with values straddling from 1.41×10^4 (Jm^{-3}) (Hirone *et al.* 1962) to 5.1×10^4 (Jm^{-3}) (Sato *et al.* 1964) with values of $K_1 = 2.83 \times 10^4$ (Jm^{-3}) (Mikami *et al.* 1959) and $K_1 = 3.5 \times 10^4$ (Jm^{-3}) (Sato *et al.* 1964).

Apart from experimental difficulties, a reason for the rather wide K_1 variability could be the absence of the ideal hexagonal configuration in pyrrhotite grains in rocks. In ideal single domain (SD) particles with triaxial anisotropy confined to a basal plane, the ratio of the remanent saturation magnetization (M_{rs}) and the saturation magnetization (M_s): $M_{rs}/M_s = 0.75$ (Dunlop & Özdemir 1997). However, this value is rarely obtained for SD pyrrhotite-bearing rocks (review in Peters & Dekkers 2003). The closest values found in nature are present in sediments with an M_{rs}/M_s ratio of approximately 0.7 (Horng & Roberts 2006) but were never reported in fractionated extracts or synthetic samples, with experimental values of the M_{rs}/M_s ratio close to 0.5 (Clark 1984; Dekkers 1988; O'Reilly *et al.* 2000).

1.2 Low-field susceptibility and anisotropy behaviour of pyrrhotite

Pyrrhotite's low-field susceptibility is notably dependent on the pyrrhotite grain size, and the fieldstrength and frequency utilized for its determination (because pyrrhotite is a semiconductor) (e.g. Dekkers 1988; Worm 1991; Worm *et al.* 1993; Pokorný *et al.* 2004). Below 1 kHz frequency of the applied field, out-of-phase phenomena can safely be ignored: the low-field susceptibility increases with the measurement field strength in the range from 10 to 2000 A m^{-1} . Large multidomain (MD) grains show this behaviour most conspicuously, SD grains barely show any dependence (Worm *et al.* 1993).

Pyrrhotite starts showing an increase in low-field susceptibility with fields at much lower fieldstrengths than (titano)magnetite which provides a tool for diagnosing pyrrhotite in rocks (Hrouda *et al.* 2006a). The corresponding Rayleigh function that represents the variation of bulk susceptibility with applied field was derived for grain size fractions of pyrrhotite by Hrouda (2002). The Rayleigh region is the field range in which the low-field susceptibility can

be described by: $M = kH + \alpha H^2$ where M is the magnetization, H is the applied field, k is the initial susceptibility and α is the Rayleigh coefficient (Neel 1942). In coarse-grained pyrrhotite, the Rayleigh region extends up to 80 A m^{-1} only (Worm *et al.* 1993; Hrouda 2002). Most commercial instruments use a measurement (rms) fieldstrength of about 300 A m^{-1} and a frequency of ~ 1 kHz (Pokorný *et al.* 2004), fully adequate for the fine-grained geomaterials but which may bias the analysis of coarse-grained material. For a complete understanding, the field behaviour with its deviations from Rayleigh's law, must be better characterized.

Also, the anisotropy of magnetic susceptibility (AMS) in pyrrhotite-bearing rocks displays a strong variation with applied field. This phenomenon is found in the principal AMS directions as well as in the anisotropy parameters (Hrouda 2002; Hrouda *et al.* 2006a). Anisotropy of remanence, for isothermal remanence magnetization (IRM) and anhysteretic remanence magnetization (ARM) also show variations with the applied field, which are argued to be related to the grain size and texture of the samples (de Wall & Worm 1993).

1.3 Rotational hysteresis

Rotational hysteresis is the energy stored by the magnetic particles when they are rotated in a magnetic field. Rotational hysteresis has been used to characterize irreversible magnetization properties such as oxidation state and/or degree of interaction between magnetic particles (Day *et al.* 1970; Schmidbauer & Keller 1994; Yoshida *et al.* 1994; Bottoni *et al.* 1999). It is calculated as one half of the integral of the torque function on one full 360° rotation. Rotational hysteresis varies when the applied magnetic field is changed (Collinson & Creer 1960; Stacey 1963). It reaches a maximum value at an applied field which depends on the anisotropy constant and coercivity of the material analysed; this maximum can therefore be used to identify the presence of certain magnetic particles in natural samples (Schmidbauer & Keller 1994; Muxworthy *et al.* 2002) or, under special conditions, the degree of oxidation (Day *et al.* 1970). The decay rate after the peak is related to the degree of interaction, type of magnetic material and/or domain state of the magnetic particles. Interaction between particles can influence the remanence behaviour of oxidized particles. It obviously plays a role in samples with a high concentration of magnetic particles. When dealing with single crystals, rotational hysteresis can provide information about the amount of doping; the area of the rotational hysteresis curve is a function of applied field with the amount of doping (Bottoni 1995). It can also be used to identify accumulation of stress, very important for the remagnetization of pyrrhotite-bearing rocks according to experiments on synthetic rocks (Robion & Borradaile 2001).

1.4 The present investigation

Single crystals are the best option to understand the magnetic anisotropic structure of pyrrhotite and the anisotropy constants that govern their structure. Therefore we selected 11 seemingly single crystals of pyrrhotite based on optical examination. These are characterized magnetically by coercivity spectrum analysis, hysteresis parameters, Curie temperature determination, and FORC diagrams. Their susceptibility anisotropy behaviour serves as a final screen for single crystal detection. Six samples were subjected to high-field torque measurement. Three crystals yielded a reliable K_1 determination for pyrrhotite for the first time. The torque magnetometer measurements also enable an in-depth analysis of the

rotational hysteresis behaviour of pyrrhotite. Further we re-evaluate existing low-field susceptibility data as a function of applied field proposing an empirical function that informs about the dominant grain size fraction.

2 SAMPLES AND METHODS

The eleven samples processed consist of two groups: pyrrhotite ore samples from which single crystals were collected (~3 mm length) and pyrrhotite single crystals (Table 1). Separate chips were selected for the initial rock magnetic characterization on the one hand and for the AMS and torque measurements on the other. Clean (no impurities visible with a binocular) grains visually being single crystals (hexagonal crystal habitus with smooth crystal faces) were cleaved from the bigger crystal aggregates. The chips selected for AMS measurements were hexagonal or close-to-hexagonal platelets (basal plane). The magnetic anisotropy of the samples is dominated by the magnetocrystalline anisotropy and the samples were close to a disk shape.

Thermomagnetic analysis was performed in air with a modified horizontal translation Curie balance (Mullender *et al.* 1993). The cycling field varied from 150 to 300 mT; heating and cooling rates were 10 °C min⁻¹. The so-called incremental heating and cooling segments protocol was used to detect chemical alteration; the final heating temperature was 650 °C. Only one sample was heated up to 700 °C; it displayed an increase in magnetization at about 420 °C followed by a decrease until 600 °C, a typical feature of the presence of pyrite. Curie temperatures were determined by the ‘*intersecting tangent*’ method from the heating transect covering the temperature range from 250 to 350 °C (Moskowitz 1981).

Hysteresis loops up to 2 Tesla were measured on a Micromag 2900 alternating gradient magnetometer (Princeton Inc., USA). From these the saturation magnetization (M_s), saturation remanence (M_{rs}), and coercive force (B_c) were extracted. Sample pyr.11 was processed on a Variable Force Translation Balance high-sensitivity magnetometer (Petersen Instrument), which has a maximum applied field of 1 T.

First-order-reversal-curve (FORC) diagrams were determined with an alternating gradient magnetometer on chips extracted from the crystals of the eleven samples. This was done to evaluate the microcoercivity distribution and magnetic interactions (Pike *et al.* 1999; Roberts *et al.* 2000; Pike *et al.* 2001). FORC diagrams were based on a set of 100 curves, a saturation field of 1000 mT, field increment of 1.36 mT and averaging time of 0.2 s, waiting time after saturation of 1 s and waiting time between subsequent data points of 1 s. The diagram was determined using a smoothing factor (SF) of two.

The alternating gradient magnetometer was used as well to determine IRM acquisition curves up to 2 T and subsequent backfield demagnetization for the determination of the coercivity of remanence (B_{cr}). Prior to the IRM acquisition, samples were AF demagnetized to acquire the same initial state (Heslop *et al.* 2004). The shape and saturation values for the IRM curve, when normalized by mass or volume, are used for the identification of the magnetic phases present in the samples (e.g. Dunlop & Özdemir 1997; Evans & Heller 2003).

Coercivity spectra are helpful in the identification of magnetic populations (Spassov *et al.* 2004) and/or their abundance (Geiss & Zanner 2006). Therefore, the IRM acquisition curves were processed by the procedures of Kruiver *et al.* (2001) and Egli (2003) to determine the number magnetic populations and their coercivity.

Table 1. Mass, saturation remanence M_r , saturation magnetization M_s , remanent coercive force H_{cr} , coercive force H_c (and B_c for comparison reasons), M_r/M_s , H_{cr}/H_c , Curie temperature T_c , B_o and B_u values of the FORC density maximum, pyrrhotite type based on thermomagnetic curves (mpo: monoclinic and hpo: hexagonal), percentage of monoclinic pyrrhotite estimated from the M_s values measured and taking the literature value for pure monoclinic pyrrhotite of $M_s = 80 \text{ kA m}^{-1}$ (e.g. Dunlop & Özdemir 1997) and sample locality and rock type. Data are normalized by volume using a mean density of 4.61 gr cm^{-3} (Lindsley *et al.* 1966). Crystals taken from pyrrhotite ores are labelled as ‘*ore*’; single crystal samples are labelled as ‘*sin. xtl*’.

Sample	Mass (mg)	M_r (kA m ⁻¹)	M_s (kA m ⁻¹)	H_{cr} (kA m ⁻¹)	H_c (kA m ⁻¹)	B_c (mT)	M_r/M_s	B_{re}/B_c	T_c (°C)	FORC		Type	Mpo (%)	Description
										B_o (mT)	B_u (mT)			
pyr.1	15.2	8.14	34.81	13.01	10.47	13.16	0.23	1.24	320	10.6	-2.2	mpo. & hpo.	43.5	loc. unknown (ore)
pyr.2	4.85	6.33	15.77	14.06	12.74	16.01	0.40	1.10	284	10.9	-2.6	mpo. & hpo	19.7	loc. unknown (ore)
pyr.3	10.4	2.96	20.60	18.77	10.46	13.14	0.14	1.79	305	13.5	-2.5	mpo. & hpo.	25.7	loc. unknown (ore)
pyr.4	15.3	8.03	64.59	4.05	2.45	3.07	0.12	1.65	324	2.8	-0.3	monoclinic	80.7	loc. unknown (ore)
pyr.5	11.6	6.22	48.32	4.90	3.10	3.89	0.13	1.58	320	2.2	0.0	mpo. & hpo	60.4	loc. unknown (ore)
pyr.6	11.5	3.75	16.83	12.32	8.82	11.08	0.22	1.40	319	4.9	-0.6	mpo. & hpo	21.0	loc. unknown (ore)
pyr.7	13.0	2.56	9.55	5.86	6.44	8.098	0.27	0.91	316	4.9	-1.0	mpo. & hpo	11.9	Potosi Mine, Mexico (sin. xtl)
pyr.8	4.71	16.83	79.07	4.99	5.29	6.65	0.21	0.94	320	4.7	-0.5	monoclinic	98.8	Minas-Gerais, Brasil (sin. xtl)
pyr.9	22.5	0.02	0.27	12.41	5.38	6.76	0.09	2.31	~	4.7	-1.0	pyrite		Quily, France (sin. xtl)
pyr.10	0.35	1.41	3.11	11.00	11.52	14.48	0.45	0.95	316	8.7	-1.7	mpo. & hpo	3.9	Isola D’Elba, Italy (sin. xtl)
pyr.11	15.4	11.06	57.5	10.14	3.31	4.16	0.19	1.60	321	6.7	-0.7	mpo. & hpo	71.9	Trepca, Yugoslavia (sin. xtl)

That of (Kruiver *et al.* 2001) is based on fitted with a series of log-Gaussian distributions. Egli's (2003) procedure is more generic and uses skewed generalized Gaussian curves as base function. Each distribution is described by its SIRM (amount, $\text{Am}^2 \text{kg}^{-1}$ when expressed on a mass-specific basis), median acquisition field $B_{1/2}$ (the mid-point of the Gaussian distribution, log mT) and dispersion parameter DP (distribution of microcoercivities, log mT). The important difference between the two approaches is that magnetic interaction and/or thermal activation that lead to skewed-to-the-left distributions (Heslop *et al.* 2004) can be dealt with in Egli's procedure assuming those features are attributed to the intrinsic properties of the samples.

Low-field magnetic susceptibility and the anisotropy of magnetic susceptibility (AMS) were measured on a KLY-4S instrument manufactured by AGICO (Brno, Czech Republic), (Pokorný *et al.* 2004; Hrouda *et al.* 2006b). The instrument has an operating frequency of 875 Hz, during the experiment the field was varied from 2 to 450 A m^{-1} (rms).

Several parameters are in use to evaluate the increment of k_{bulk} with applied field. de Wall & Nano (2004) proposed the difference in susceptibility measured at 300 and 30 A m^{-1} scaled to the 30 A m^{-1} value and expressed as a percentage (V_{LF}). Hrouda *et al.* (2006a) proposed to use the entire field range available on the KLY-4, that is, the difference in susceptibility measured at 450 and 2 A m^{-1} is scaled to the 2 A m^{-1} value and again expressed as a percentage (V_p).

$$V_{LF} = 100 \frac{k_{300} - k_{30}}{k_{30}}$$

$$V_p = 100 \frac{k_{450} - k_2}{k_2}. \quad (1)$$

The full AMS tensor was computed with the multivariate analysis approach (Jelinek 1978b); the 'Ellipsoid software' is used for the graphical representation and mean values on the Jelinek plot (Launeau & Robin 2005).

The AMS ellipsoid principal directions are computed using for each applied field the statistical methods of Jelinek (1978a). Hrouda *et al.* (2006a) proposed a fabric index to characterize the maximum susceptibility variation with field, defined as follows:

$$V_m = 100 \frac{k_{\text{max}} - k_{\text{min}}}{k_{\text{min}}}, \quad (2)$$

where k_{max} is the maximum susceptibility semiaxis and k_{min} is the minimum susceptibility semiaxis. Here we have taken only the mea-

surement at the standard 300 A m^{-1} into consideration for illustration and comparison with reported values.

The magnetocrystalline anisotropy in the pyrrhotite single crystals was determined with a high-field cantilever magnetometer by evaluating the magnetic torque as function of angle in various applied magnetic fields. The instrument and measurement procedure are described by Martín-Hernández *et al.* (2006). The magnetic torque in the basal plane was measured in a set of fields ranging from 0 to 2 T in both senses, clockwise and counter-clockwise. Mikami *et al.* (1959) derived the following torque expression from the magnetic energy function for intermediate fields:

$$T(\theta) = -\frac{3}{2} \frac{K_1^3}{B^2 M_s^2} \left(1 - 2 \frac{K_1^2}{B^2 M_s^2}\right) \sin(6\theta) + 10 \frac{K_1^6}{B^5 M_s^5} \sin(12\theta), \quad (3)$$

where T is the measured torque, θ is the angle that describes the rotation of the sample, K_1 is the first anisotropy constant, B is the applied field and M_s is the saturation magnetization of pyrrhotite. The rotational hysteresis, defined as one half the integral of the torque for one field over a full rotation, is computed practically as the area enclosed by the torque function when the sample is rotated clockwise and counter-clockwise in for each applied fieldstrength (Bozorth 1951; Day *et al.* 1970; Muxworthy 2002).

3 ROCK MAGNETIC CHARACTERIZATION OF THE PYRRHOTITES

3.1 Thermomagnetic runs

Monoclinic (4C) pyrrhotite (Fig. 1a), hexagonal (NC) pyrrhotite (Fig. 1b) showing the λ -transition at $\sim 215^\circ\text{C}$ (phase change to NA pyrrhotite) with its upper bound at $\sim 265^\circ\text{C}$ (Kissin & Scott 1982) although it can be higher (change to MC pyrrhotite which is antiferromagnetic again) and mixtures of both pyrrhotites occur (Fig. 1c). Note that upon heating over $\sim 500^\circ\text{C}$ magnetite starts to form. The pyrrhotite phase(s) identified and Curie temperatures are collected in Table 1; this should be considered with some caution since over 95 per cent of the pyrrhotites consists of intergrown monoclinic-hexagonal pyrrhotite (Arnold (1967). The Curie temperature of 4C pyrrhotite is ~ 310 – 320°C determined on the heating segments before the onset of magnetite formation (Table 1). The 'Curie temperature' of the hexagonal pyrrhotite sample is somewhat lower at

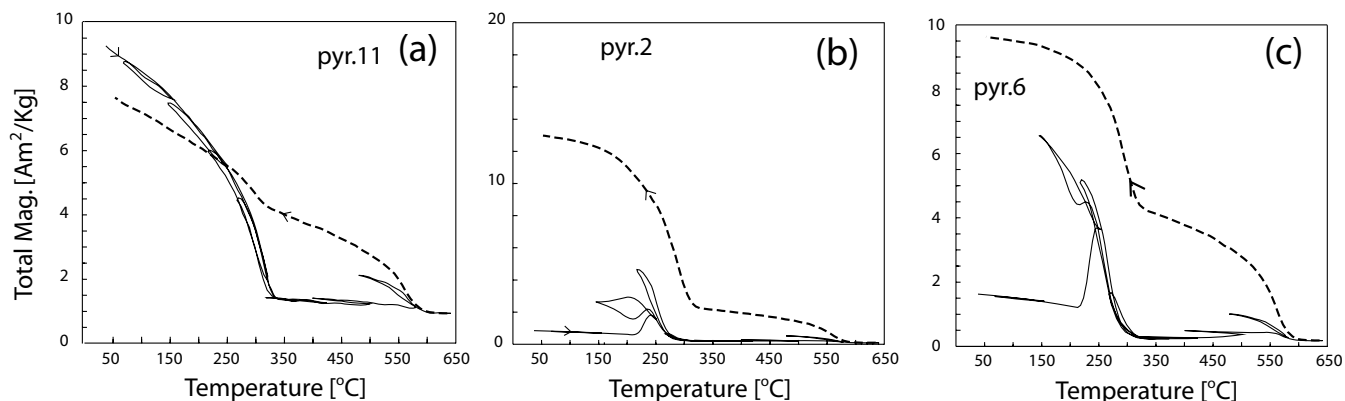


Figure 1. Representative thermomagnetic runs showing the three characteristic pyrrhotite features. Solid lines correspond to the warming curves and dashed lines to the final cooling curves. (a) monoclinic pyrrhotite, (b) hexagonal pyrrhotite displaying the characteristic ' λ -transition' and (c) mixture of hexagonal and monoclinic pyrrhotite.

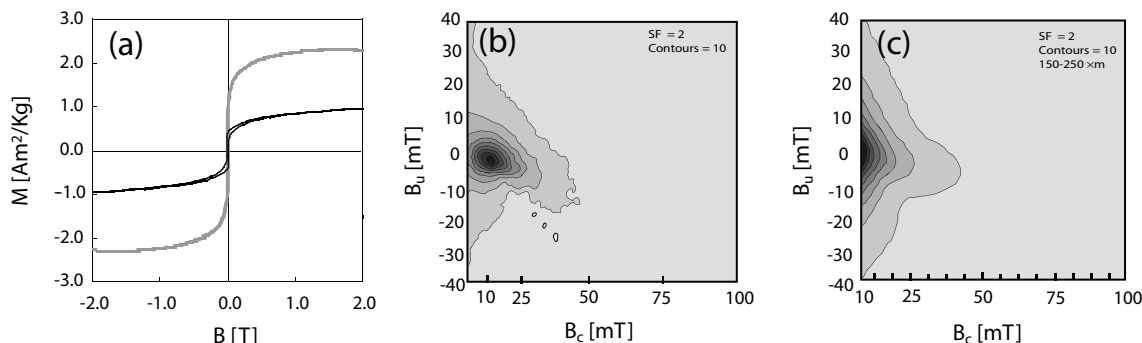


Figure 2. (a) Hysteresis loops in applied fields up to 2 T for a typical pyrrhotite single crystal (sample pyr.7 in grey shading) and for a pyrrhotite single crystal displaying a wasp-waisted shaped loop (sample pyr.10 in black); (b) FORC diagram acquired for sample pyr.1; and (c) FORC diagram of the grain size fraction 150–250 μm (Wehland *et al.* 2005). Note that the diagram is clipped close to the origin because of incomplete grids close to $B_c = 0$.

~ 280 – 290 $^{\circ}\text{C}$ (Fig. 1b). That of the mixed (hybrid) sample is ~ 320 $^{\circ}\text{C}$ (Bennett & Graham 1980) (Fig. 1c).

3.2 Hysteresis parameters and FORC diagrams

Hysteresis loops and FORC diagrams were measured parallel to the pyrrhotite basal plane. They are similar in shape and characteristics for all samples. Two typical examples are shown in Fig. 2(a). Saturation is reached in most of the samples by 600 mT. Some samples seem to be magnetically harder and saturation is not fully achieved by 2 T. Occasionally, the loop remains open in fields up to 1 T which yields a typical wasp-waisted shape (Fig. 2a). This feature is indicative of the presence of two phases with notably different coercivities (Roberts *et al.* 1995; Tauxe *et al.* 1996). The origin of the second or high-coercivity component is explained in Section 3.3 but we anticipate here that it might be caused by small misorientation of the basal plane (which is delicate). The projection of the hard magnetization axis (c -axis) would give an apparent high-coercivity phase.

Calculation of M_s following the ‘*approach to saturation*’ procedure outlined by Fabian (2006) led to similar values compared to the results without the approach to saturation, with variations smaller than 5 per cent with one exception. Sample pyr.11 was measured up to 1 T. For this sample, the differences between the two M_s values reached 17 per cent and therefore only the higher ‘*approach to saturation*’ value is reported. M_{rs}/M_s ratios vary from ~ 0.12 to ~ 0.45 and B_{rc}/B_c from ~ 0.91 to 2.31 (Table 1). The B_{rc}/B_c ratio is also smaller than 1.5 for most of the samples, typical of pyrrhotite and pyrrhotite-bearing rocks (Peters & Dekkers 2003). The percentage of monoclinic pyrrhotite (Table 1) was estimated based on the reported value of $M_s = 80 \text{ kA m}^{-1}$ for pure monoclinic pyrrhotite (e.g. Dunlop & Özdemir 1997). Even though in some samples the thermomagnetic curves did not indicate hexagonal pyrrhotite, the estimation of monoclinic pyrrhotite is not 100 per cent, suggesting minor amounts of hexagonal intergrowths.

To track possible variations in the interaction field of the samples, FORC diagrams were determined (Fig. 2b). The coercivity shown on the diagrams is compatible with the largest MD pyrrhotite fraction which has been experimentally determined by Wehland *et al.* (2005) (Fig. 2c). The contour lines on the vertical axes for the single crystals are closer spaced than those of the fractionated samples, suggesting a less pronounced MD behaviour for the single crystals. This is likely because we are dealing with single crystal samples (or almost single crystal samples) that were measured within the basal plane. Evidently this is not a randomly dispersed sample. The shape of the FORC diagram shows some similarities with that of

a SD state, which obviously cannot be present (crystals are large and coercivity values are too low). The asymmetry of the contour lines on the vertical axes is larger in the single crystals (Fig. 2b). This phenomenon is indicative of a larger interaction field, probably an interaction within the crystal lattice (Pike *et al.* 2001). Accumulation of stress within the crystal lattice or misorientation of the basal plane on the measurements can also produce asymmetry on the diagram. Here this asymmetry (when mirrored around the $B_u = 0$ axis) is larger than the general asymmetry of FORC diagrams which appears intrinsically due to the measurements (Muxworthy *et al.* 2005).

Polycrystalline pyrrhotite ore samples have slightly larger value of the coercivity within the MD state (Table 1). Values of B_c determined from hysteresis loops and from the FORC diagrams are proportional, with determinations derived from FORC diagrams being slightly lower: they appear to be ~ 0.97 times those from the major hysteresis loops (Table 1).

3.3 IRM acquisition curves and coercivity spectra

The IRM acquisition curves are similar for all samples, with an inflection point at about 200 mT and a monotonous small increase of magnetization from 600 mT to 2 T (Fig. 3a). The median acquisition field ($B_{1/2}$) and dispersion parameter (DP) for the calculated distributions using the Kruiver *et al.* (2001) and Egli (2003) methods are summarized in Table 2. As a rule, the coercivity spectrum is fitted with one main distribution of medium coercivity evidently attributed to the pyrrhotite crystal (Fig. 3b). The fitted properties of the main component are independent of the fitting method used (within uncertainty range; Table 2): A mean of 17 ± 7 mT for $B_{1/2}$ and a DP of $0.32 \pm 0.05 \log \text{ mT}$ are obtained using the Kruiver *et al.* (2001) approach while Egli’s (2003) approach yields 19 ± 8 mT for $B_{1/2}$ and $0.34 \pm 0.06 \log \text{ mT}$ for DP. Fig. 3(b) illustrates the coercivity fit of a pyrrhotite single crystal. In some samples, a soft component is also present, with varying intensities (Table 2). It is attributed to thermal relaxation and/or magnetic interaction (Heslop *et al.* 2004). In large single crystals, the second is more likely to happen.

The main difference between the two approaches is how a third component of high coercivity is modelled in some samples. This component is more often required in the fitting with symmetric distributions (Kruiver *et al.* 2001). However, the DP associated with that high coercivity component using both methods (> 1.0) is unrealistically high for a single magnetic population. Therefore, this component is probably related to the orientation of the crystal during

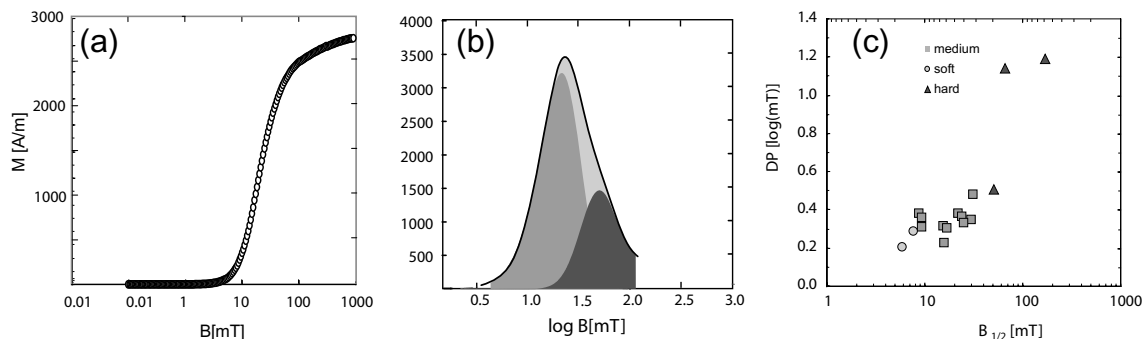


Figure 3. (a) IRM acquisition curve of sample pyr.1; (b) coercivity spectra derived from (a) (main component: medium grey, high-field component: dark grey, total: light grey) and (c) summary of all the coercivity components found in the eleven analyzed pyrrhotite single crystals (only components with percentages of intensity larger than 3 per cent are displayed). Egli's (2003) software was used.

measurement (the hard component is caused by acquisition of remanent magnetization along the c -axis, the hard magnetic axis).

4 LOW-FIELD BULK SUSCEPTIBILITY

The mean bulk susceptibility was evaluated as the mean of the three magnetic AMS ellipsoid axes at 300 A m^{-1} , $k_{\text{bulk}} = (k_{\text{max}} + k_{\text{int}} + k_{\text{min}})/3$. The bulk susceptibility is expressed on a volume specific basis by taking the measured mass and dividing by a value of 4.61 gr cm^{-3} being the specific density of pyrrhotite (Lindsley *et al.* 1966). The bulk susceptibility displays a large variation in spite of samples being selected and thoroughly cleaned before.

V_p and V_{LF} show a rather large between-sample variation, V_{LF} ranges from 1 to 70 per cent and V_p from 4 to 85 per cent (Table 3). This variation can reach values even up to 200 per cent when the magnetic susceptibility was measured only in one direction within the basal plane and not averaged out over all directions.

The k_{bulk} at low fields can be fitted to a Rayleigh law curve (see Section 1). However, for pyrrhotite-bearing rocks the field interval in which the fitting is reasonable, varies depending on the pyrrhotite type and concentration, reaching 450 A m^{-1} only in some cases (Hrouda *et al.* 2006a). The region in which pyrrhotite obeys the Rayleigh law is up to about 80 A m^{-1} (Hrouda *et al.* 2006a). However when measuring low-field susceptibility, the most commonly used field is 300 A m^{-1} , which guarantees an optimal signal to noise ratio (e.g. Jelinek 1973). For a pyrrhotite single crystal, Fig. 4(a) illustrates the values obtained for the Rayleigh law fitting using all data from 2 to 450 A m^{-1} and data in the field range from 2 to 300 A m^{-1} as suggested by Hrouda (2002). The results illustrate that for pyrrhotite single crystals and probably pyrrhotite-bearing rocks as well; the most common fields used are already in the so-called 'minor loop' region and (far) beyond the Rayleigh region.

The values of k_{bulk} appear to be dependent on the logarithm of the applied field. They can be fitted with the following polynomial:

$$k_{\text{bulk}} = a_2 [\log(H)]^2 + a_1 \log(H) + a_0, \quad (4)$$

where a_2 , a_1 and a_0 are the coefficients of the fitting and H is the applied field in A m^{-1} .

The scalar a_0 cannot be related only to the pyrrhotite crystals but also to paramagnetic material and/or magnetite when present in the samples. At room temperature, paramagnetic minerals have a constant magnetic susceptibility with applied field up to several hundreds of Teslas. For the field range used, magnetite is also independent in the field ranged used here (Worm 1991; Worm *et al.* 1993; Hrouda 2002). The relationship expressed in eq. (4) is illus-

trated in Fig. 4(b) for sample pyr.1; the fitted coefficients and the goodness of fit statistics R_{pol}^2 are displayed on the figure.

Eq. (4) was applied to the grain size fractionated data set measured by Worm *et al.* (1993). Fig. 5(a) shows the magnetic susceptibility of fractions labelled 'EOR' fitted to eq. (4). The second order coefficients (a_2) of the polynomial described by eq. (4) for all data are summarized in Fig. 5(b). The first order coefficients (a_1) are reported in Fig. 5(c). There is a clear correlation between the coefficients of the polynomial and the grain size of the pyrrhotite (Table 4, Figs 5b and c). Values of a_2 increase with grain size while a_1 values decrease with increasing grain size. Only the behaviour of sample TTE250 does not concur with the others (Figs 5b and c). This is attributed to intergrown pyrite by Worm *et al.* (1993).

The same data set has been fitted to a Rayleigh law function and the results are summarized in Table 4. The field range from 2 to 300 A m^{-1} has been used. The fitting is good (R_{Ray}^2 close to 0.9 for grain sizes larger than $40 \mu\text{m}$). However the fitting is systematically better for all grain sizes if eq. (4) is used instead (R_{pol}^2).

5 LOW-FIELD AMS

The eleven crystals show a widespread AMS behaviour as function of applied field in range from 2 to 450 A m^{-1} , both with respect to stability of its principal directions and to the parameters of shape and degree of anisotropy (Fig. 6 and Table 3). Four samples (pyr.2, pyr.5, pyr.7 and pyr.11) have oblate AMS ellipsoids (Figs 6a and b) with very well defined principal directions (Fig. 6a) and very high values of P' (Fig. 6b). Other samples (pyr.6 and pyr.9) have an oblate AMS ellipsoid with a well defined mean and k_3 perpendicular to the basal plane (Table 3 and Fig. 6c) but medium values of the degree of anisotropy (Fig. 6d). Again, in others (pyr.1, pyr.3, pyr.4, pyr.8 and pyr.10), the shape of the AMS ellipsoid is neutral or very close to neutral or even negative (Table 3 and Fig. 6e), contrary to the expected oblate shape. Those samples also display low values of the anisotropy degree, except for sample pyr.8+ (Table 3 and Fig. 6f).

Samples pyr.8 and pyr.10 display a susceptibility tensor has negative minimum susceptibility semiaxes and therefore the parameters P' and T cannot be computed unless a common number is added to the susceptibility eigenvalues, which was done in our study (Table 3). On these samples the parameters F and P also present negative values. This phenomenon has been already reported for hematite single crystals: because the ellipsoid is perfectly oblate, the actually measured value is not negative but the problem arises from the non-linearity between M and H (Martín-Hernández

Table 2. Component fitting results of the IRM acquisition curves after Kruijer *et al.* (2001) and Egli (2003). Absolute (S)IRM at 2 T, $B_{1/2}$ (median acquisition field) is in mT and DP (dispersion parameter) is in log mT. Mean values are followed by the standard deviation of the mean. Percentage of each component is based on amount of total intensity; components with amounts <3 per cent are not taken into account.

Sample	Kruijer <i>et al.</i> (2001)												Egli (2003)					
	Soft			Medium			Hard			Soft			Medium			Hard		
	$B_{1/2}$	DP	per cent	$B_{1/2}$	DP	per cent	$B_{1/2}$	DP	per cent	$B_{1/2}$	DP	per cent	$B_{1/2}$	DP	per cent	$B_{1/2}$	DP	per cent
pyr.1	2.75			19.1	0.28	75	75.9	0.64	25	15.9	0.23	65	51.1	0.51	35			
pyr.2	8.6×10^7			19.1	0.28	75	74.1	0.60	25	22.1	0.38	100						
pyr.3	0.63			27.2	0.27	69	125.9	0.65	30	30.2	0.35	97						
pyr.4	2.0			9.1	0.37	98				8.8	0.38	100						
pyr.5	1.9			9.1	0.28	97				7.7	0.29	34						
pyr.6	0.86			16.6	0.27	64	89.1	0.58	33	15.6	0.32	52	65.8	1.14	48			
pyr.7	0.76			10.0	0.35	94				17.1	0.30	54						
pyr.8	5.1			9.8	0.29	96				9.5	0.31	100						
pyr.9	5.5×10^{-3}	4.0	0.28	7	0.30	85	100.0	0.30	8	23.8	0.37	100						
pyr.10	0.184	7.9	0.15	25	0.37	50	794.3	1.05	25	24.9	0.33	52	167.9	1.19	45			
pyr.11	0.0228			25.1	0.40	84	100.0	0.30	13	31.1	0.48	97						
Mean		6.0 ± 2.8	0.22 ± 0.09	17 ± 7	0.32 ± 0.05		214 ± 285	0.6 ± 0.3		7 ± 1	0.2 ± 0.1		19 ± 8	0.34 ± 0.06	65	95 ± 64	0.9 ± 0.4	

Table 3. Low-field bulk susceptibility at 300 A m^{-1} , field dependence parameters V_{LF} and V_p , variation of the maximum susceptibility index V_m (Hrouda *et al.* 2006a), magnetic lineation (L), magnetic foliation (F), degree of anisotropy (P), corrected degree of anisotropy (P') and shape parameter (T) (Jelinek 1978a) and major semi-axis (a_{ij}) and minor semi-axis (b_{ij}) of the uncertainty ellipses (α_{ij}) for the AMS mean values using the statistical procedure proposed by Jelinek (1978a).

Sample	k_{bulk} (SI)	V_{LF}	V_p	V_m	L	F	P	P'	T	α_{12}			α_{13}			α_{23}		
										a_{12}	b_{12}	α_{12}	a_{13}	b_{13}	α_{13}	a_{23}	b_{23}	α_{23}
pyr.1	2.56×10^{-1}	38.0	59.5	224	1.118	1.166	1.304	1.309	0.192	1.9	0.5	2.5	1.9	2.5	0.4	0.4	0.4	0.4
pyr.2	0.20×10^{-1}	31.5	12.4	830	1.050	8.857	9.297	12.770	0.956	32.6	1.5	32.6	0.6	1.6	0.9	0.9	0.9	0.9
pyr.3	0.62×10^{-1}	6.9	9.0	31	1.103	1.092	1.204	1.204	-0.057	0.9	0.7	7.1	0.6	7.1	0.6	7.1	0.6	0.6
pyr.4	0.59×10^{-1}	35.7	54.3	276	1.029	1.755	1.807	1.949	0.902	7.6	6.0	7.6	4.6	5.5	1.1	1.1	1.1	1.1
pyr.5	6.08×10^{-1}	70.7	84.0	4284	1.166	37.598	43.843	72.200	0.919	9.4	2.1	9.5	2.0	2.3	2.0	2.0	2.0	2.0
pyr.6	0.20×10^{-1}	44.7	54.8	492	1.043	3.054	3.185	3.344	0.945	22.3	1.4	22.2	1.0	1.7	0.7	0.7	0.7	0.7
pyr.7	0.45×10^{-1}	37.3	40.9	2883	1.354	22.022	29.818	42.846	0.821	4.0	1.0	4.0	0.6	1.3	0.2	0.2	0.2	0.2
pyr.8	2.10×10^{-1}	46.4	62.8	-17.26	1.476	-241.77	-356.96	2.657	0.488	2.3	1.2	2.1	0.8	1.8	0.2	0.2	0.2	0.2
pyr.9	0.60×10^{-1}	1.7	4.0	60	1.012	1.448	1.466	1.564	0.963	51.7	2.2	51.7	1.1	2.3	1.2	1.2	1.2	1.2
pyr.10	0.03×10^{-1}	1.1	18.5	-659	1.673	-3.340	-5.588	3.289	0.568	4.1	0.8	4.1	1.5	1.5	0.8	0.8	0.8	0.8
pyr.11	8.50×10^{-1}	33.7	56.5	8509	1.121	30.724	34.429	55.826	0.936	2.1	0.3	2.1	0.3	0.3	0.3	0.3	0.3	0.3

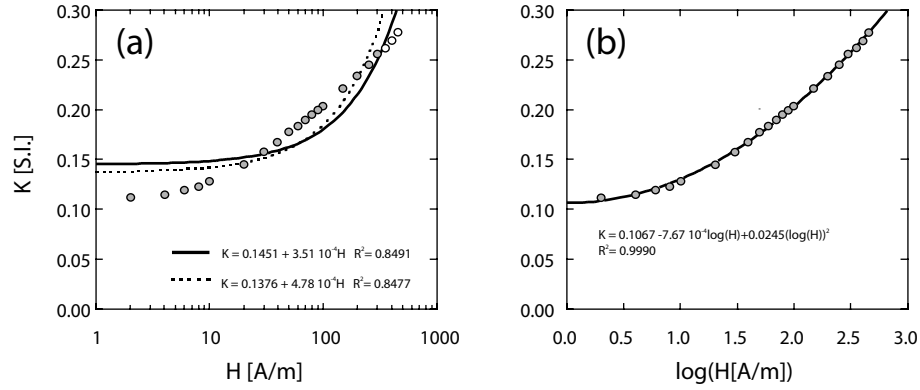


Figure 4. Low-field bulk susceptibility as a function of applied field for pyrrhotite single crystal pyr.11. (a) Susceptibility fitted to the Rayleigh law for all data points (full line) and for those ranging from 2 to 300 A m^{-1} (dotted line and grey circles). Note the logarithmic scale of the abscissa. (b) Susceptibility as function of the logarithm of applied field H (A m^{-1}) and the fitted second order polynomial. The fitted equations and their goodness-of-fit coefficients (R^2) are shown on the panels. The abscissa is logarithmic.

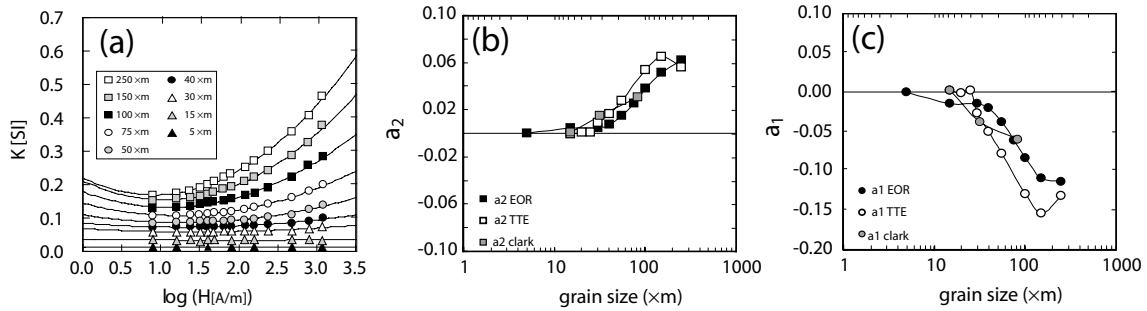


Figure 5. (a) Low-field bulk susceptibility as a function of applied field for several grain size fractions of EOR pyrrhotite (Worm *et al.* 1993). Panels (b) and (c) Summary of the polynomial coefficients in eq. (4) for all grain size dependent data reported in the literature. These are the data from series EOR (displayed in panel (a)), series TTE and data from Clark (Worm *et al.* 1993). Panel (b) shows the results for the quadratic or second order coefficient and (c) those for the linear or first order coefficient.

Table 4. Coefficients for the fitting of the data reported by Worm *et al.* (1993) to eq. (4) (a_2 and a_1) with the goodness of fit parameter R_{pol}^2 and to the Rayleigh law function (α , k) together with the goodness of fit parameter R_{Ray}^2 for the second function.

Sample	Grain size (μm)	a_2	a_1	R_{pol}^2	k	α	R_{Ray}^2
EOR	250	0.0617	-0.1130	0.9983	0.174	0.000582	0.9566
EOR	150	0.0518	-0.1088	0.9970	0.155	0.000404	0.9667
EOR	100	0.0378	-0.0834	0.9960	0.132	0.000261	0.9747
EOR	75	0.0253	-0.0611	0.9967	0.107	0.000100	0.9899
EOR	55	0.0147	-0.0370	0.9766	0.087	0.000070	0.9613
EOR	40	0.0075	-0.0192	0.9727	0.072	0.000040	0.9378
EOR	30	0.0047	-0.0137	0.9035	0.059	0.000010	0.6727
EOR	15	0.0047	-0.0137	0.9035	0.033	0.000006	0.0348
EOR	5	3.010^{-5}	0.0004	0.7141	0.012	0.000003	0.2400
TTE	250	0.0563	-0.1309	0.9911	0.188	0.000396	0.9867
TTE	150	0.0649	-0.1527	0.9942	0.240	0.000404	0.9825
TTE	100	0.0534	-0.1282	0.9892	0.231	0.000300	0.9863
TTE	55	0.0279	-0.0772	0.9876	0.204	0.000100	0.9039
TTE	40	0.0167	-0.0491	0.9512	0.182	0.000030	0.8469
TTE	30	0.0092	-0.0256	0.9603	0.183	0.000030	0.7700
TTE	25	0.0011	0.0033	0.9185	0.158	0.000050	0.7431
TTE	20	0.0007	-0.0009	0.5957	0.128	0.000008	0.2370
TTE	15	-0.0007	0.0030	0.0790	0.023	0.000008	0.0451
Clark	83	0.0304	-0.0590	0.9952	0.181	0.000300	0.9760
Clark	32	0.015	-0.0376	0.9453	0.115	0.000070	0.9108
Clark	15	0.0006	0.0028	0.9631	0.083	0.000030	0.7953

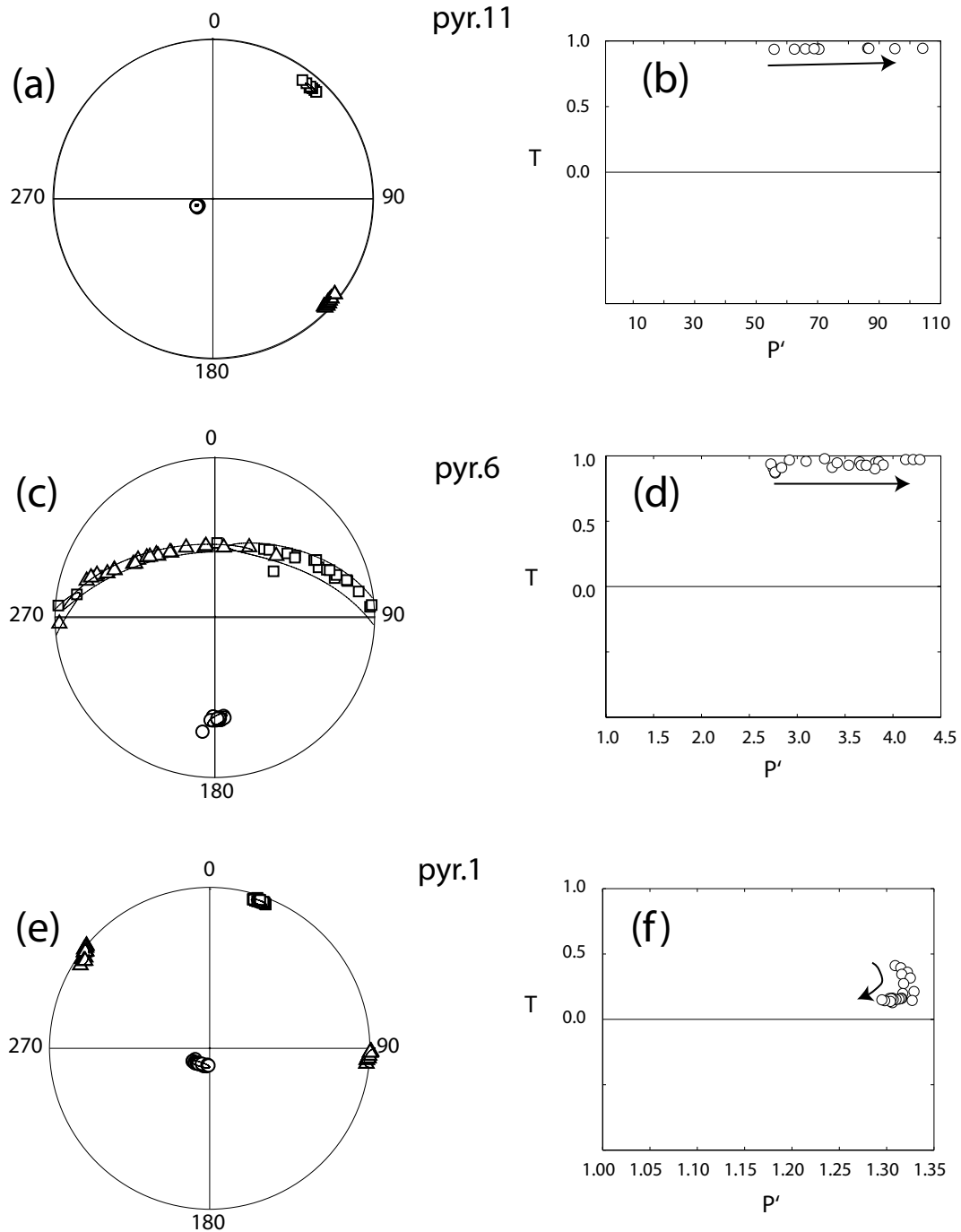


Figure 6. Principal directions of AMS (left-hand side) and corresponding Jelinek plot (right-hand side) for pyrrhotite crystals displaying three types of behaviour with low field AMS evaluated at different field strengths ranging from 2 to 450 A m⁻¹. Stereogram in specimen coordinates with the *c*-axis subparallel to the minimum susceptibility direction, lower hemisphere projection. The arrows indicate increasing applied field values: (a) and (b) Sample pyr.11: stable AMS principal directions, oblate AMS ellipsoid and high degree of anisotropy, (c) and (d) Sample pyr.6: k_1 and k_2 semiaxes dispersed on a great circle while a purely oblate AMS ellipsoid is expected but lower anisotropy degree, (e) and (f) Sample pyr.1: stable principal ellipsoid directions but anomalously low shape parameter T of the AMS ellipsoid and low degree of anisotropy. The arrow indicates the trend toward increasing values of the applied field.

& Hirt 2004). The susceptibility matrix contains either negative or two equal eigenvalues. The measurements cannot be fitted to a triaxial ellipsoid because it degenerates into a plane (Hrouda 2002).

V_m values show a rather large variation from -659 to 8509 (Table 3). Sample pyr.11 has an anomalously high value, higher than the higher reported value of 230 (Hrouda *et al.* 2006a).

6 HIGH-FIELD TORQUE MAGNETOMETRY

The delicate high-field torque measurements were performed on six (pyr.2, pyr.7, pyr.8, pyr.9, pyr.10 and pyr.11) of the eleven samples, only those suitable to be mounted on the cantilever. Three out of

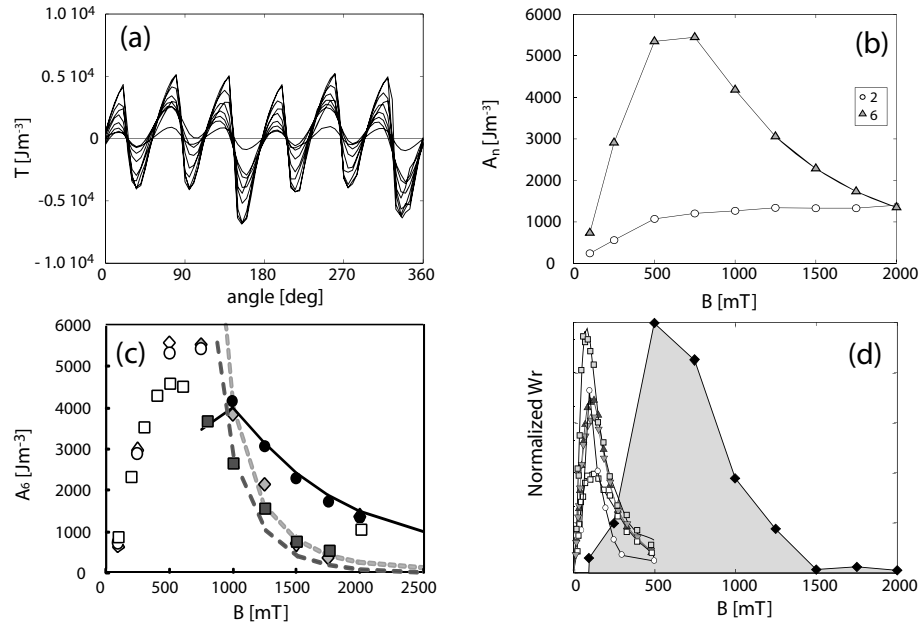


Figure 7. Cantilever torque measurements and main derived parameters. (a) Mean torque curve of a pyrrhotite single crystal within the basal plane (pyr.11), (b) dominant Fourier coefficients of the torque signal (pyr.11), (c) 6θ term (A_6) of the curve and fitted theoretical expression (eq. (3)) where full symbols present the data points selected to fit the curve into its theoretical expression for all the new samples analyzed in this study. Diamonds and light-dotted grey curve correspond to pyr. 7, squares and dark-dotted grey line correspond to pyr.2 and circles and black line correspond to pyr.11. (d) Rotational hysteresis of pyrrhotite single crystal pyr.11 (black diamonds) compared with the rotational hysteresis of magnetite for different grain sizes (grey squares, $7.5 \mu\text{m}$; black triangles, $39 \mu\text{m}$; grey triangles $59 \mu\text{m}$ and open squares, $79 \mu\text{m}$, all from Muxworthy (2002) and open circles magnetite single crystals from Martín-Hernández *et al.* (2006)).

these six crystals (pyr.2, pyr.7 and pyr.11) showed an interpretable torque signal attributable to the pyrrhotite basal plane only. The other three had either a significant contribution of a second overlapping phase which increased the torque amplitude up to fields higher than 2 T or the signal was too weak to be measured.

As expected, the torque curve is dominated by a 6θ term (Fig. 7a). This term increases in magnitude until a maximum value at 600 mT, the field in which pyrrhotite magnetization saturates when measured within the basal plane (Fig. 7b). For fields higher than 600 mT, the 6θ term decreases to zero. A more extended analysis shows a superposition of a 6θ and 2θ term for the entire field range. The presence of an overlapping 2θ term to the theoretical 6θ curve is already described for pyrrhotite single crystals, most likely due to a small misorientation of the crystal (Mikami *et al.* 1959; Hirone *et al.* 1962). By a non-linear least squares fitting, the 6θ coefficient of the torque curve can be fitted to eq. (3) with K_1 as the only unknown parameter. The value of K_1 can then be derived (Fig. 7c). M_s values for the different samples have been taken from the hysteresis measurements (Table 1). Table 5 summarizes in the first column values reported in the literature evaluated by torque magnetometry (Mikami *et al.* 1959; Hirone *et al.* 1962) and magnetization curves (Bin & Pauthenet 1963; Sato *et al.* 1964) and in the second column values determined in the present contribution and a re-evaluation of the data reported based on torque magnetometry. Combining those five entries results in a mean value of K_1 : $(2.7 \pm 0.2) 10^4 \text{ Jm}^{-3}$.

Pyrrhotite single crystals possess a maximum value of the rotational hysteresis at about 600 mT, that decays to zero monotonously at a rate proportional to $1/B$ (Fig. 7d). The peak in rotational hysteresis occurs at distinctly higher field values for pyrrhotite than for magnetite (Schmidbauer 1988; Muxworthy 2002) and titanomagnetites (Schmidbauer & Keller 1994; Keller & Schmidbauer 1999)

Table 5. Values of the first anisotropy constant (K_1) for pyrrhotite reported in the literature (first column) and data presented in this study (second column) and measured M_s values for the analysed samples (third column). Error bars in the mean correspond to the standard deviation of mean values.

Sample	K_1 (Jm^{-3})	K_1 (Jm^{-3})	M_s (kA m^{-1})
pyr.2		2.89×10^4	15.77
pyr.7		2.85×10^4	9.55
pyr.11		2.40×10^4	57.5
Mikami <i>et al.</i> (1959)	2.83×10^4	2.82×10^4	
Hirone <i>et al.</i> (1962)	1.41×10^4	2.76×10^4	
Bin & Pauthenet (1963)	3.5×10^4		≈ 97
Sato <i>et al.</i> (1964)	5.1×10^4		57
Mean		$(3.2 \pm 1.5) 10^4$ ($2.7 \pm 0.2) 10^4$	

but at lower values than hematite (Owens 1981). Since the field at which the maximum magnetic energy is stored is different for some of the most common minerals, this parameter might be used to estimate the magnetic phases in natural samples and evaluate the degree of interaction between particles (Yoshida *et al.* 1994). The existing rotational hysteresis database is too sparse to allow for robust inferences concerning the influence of grain size with respect to rotational hysteresis (Muxworthy 2002) or the accumulation of stress into the crystallographic structure (Robion & Borradaile 2001).

7 DISCUSSION AND CONCLUSIONS

7.1 Bulk susceptibility and applied field

The bulk susceptibility variation with applied field shows considerable scatter among different samples. The V_p and V_{LF} parameters display larger values when the measurements are confined to

the basal plane. This might become problematic when measuring natural samples: if the bulk susceptibility that much orientation-dependent, its variations could erroneously be attributed to other phenomena than intrinsic anisotropy of the magnetic particles. Two samples from the same site and same characteristics might have a different value of the V_p and V_{LF} if measured in the foliation plane or the pole to bedding plane, only due to the differences of anisotropy in pyrrhotite, but not attributable to variations in concentration or grain size.

In order to compare some of these parameters between different magnetic minerals, the reported pyrrhotite V_m values range from 229.6 to 2.1 in natural samples (Hrouda *et al.* 2006a) and from 8509 to -659 in single crystals (Table 3). For single domain magnetite the values range from 12.5 to 4.4 and for multidomain hematite from 9.6 to 0.9 (Hrouda *et al.* 2006a). High values may be taken as indication for the presence of pyrrhotite in the rock under investigation but values <13 can indicate several magnetic minerals.

An increasing magnetic susceptibility with applied field has also been found for titanomagnetite (Jackson *et al.* 1998; de Wall & Nano 2004) and hematite (Hrouda 2002). However, the field dependency determined for those minerals does not fit the curve proposed in this study for pyrrhotite. For this reason, caution must be taken in using the coefficients of the fitting between logarithm of applied field and bulk susceptibility as grain size estimation for pyrrhotite-bearing samples. Such samples have to fulfil two criteria for being applicable: (i) they must be devoid of titanomagnetite and/or hematite and (ii) they must contain only one population of pyrrhotite. If the samples contain hematite and/or titanomagnetite, variation of the bulk susceptibility with applied field also occurs. When more than one population of pyrrhotite is present, the function governing the correlation between applied field and susceptibility is a combination of the different populations of pyrrhotite and the interpretation would not be unique. The presence of pure magnetite, paramagnetic or diamagnetic minerals should not be a problem because their susceptibility is field-independent for the applied field range (Hrouda 2002). The results obtained so far are encouraging, but more data from other magnetic minerals are needed to confirm the universality of the relationship between grain size and applied field using a polynomial of the logarithm of applied field.

7.2 Low field AMS

The variation of susceptibility, characterized by the V_{LF} and V_p parameters does not show any correlation with the pyrrhotite composition determined by magnetic methods (Tables 1 and 3). We have analysed samples from monoclinic, hexagonal and hybrid composition in this study. Moreover, the AMS of pyrrhotite crystals is not straightforward at low fields. Some crystals showed a susceptibility ellipsoid with negative minimum susceptibility and positive maximum and intermediate susceptibility. This leads to an incorrect estimation of the susceptibility increments as expressed with the field parameter V_m . Also shape and degree of anisotropy of the ellipsoid can be calculated erroneously.

The evaluation of the main low-field AMS parameters (T and P') allows also the discrimination between 'pure' single crystal and polycrystalline specimens. Samples with low or negative values of the shape parameter T are not compatible with monoclinic pyrrhotite and therefore are the consequence of crystal aggregates. Samples displaying low to negative values of T coincide with those in which the degree of anisotropy is lower than 3 (Table 3). Low values of T and P' are interpreted to be due to a poly-

crystalline nature of the samples. AMS measurements are therefore a useful tool in the discrimination of pure single crystals from aggregates.

7.3 Magnetocrystalline anisotropy constant

High-field torque magnetometry was used for the evaluation of the anisotropy constant within the pyrrhotite basal plane. Literature values are rather dispersed, in part because different measurement techniques were used (torque magnetometry and magnetization curves). Also different theoretical developments were utilized for the same measurement. Torque data by Mikami *et al.* (1959) are based on the full torque curve while Hirone *et al.* (1962) concentrated on the torque amplitude as a function of applied field.

Previously reported works did not include a compositional analysis of the pyrrhotite. Mikami *et al.* (1959) and Hirone *et al.* (1962) use the value of $M_s = 80 \text{ kA m}^{-1}$, thus assuming that their crystals were pure monoclinic pyrrhotite. Bin and Pauthenet (1963) reported a value of $M_s \approx 97 \text{ kA m}^{-1}$, larger than the accepted value for pure monoclinic pyrrhotite. However, their value of the magnetocrystalline anisotropy constant is not the largest reported value, which was given by Sato *et al.* (1964). Their saturation magnetization appears to be 57 kA m^{-1} , ~ 40 per cent smaller than the expected value, which they commented was due to non-magnetic impurities that led to an smaller value of M_s with no demonstrable effect on the crystallographic properties (Table 5).

A re-evaluation of the data determined by torque magnetometry was done after digitizing the torque curves and fitting the results to the theoretical expression given by eq. (3). The newly evaluated values and three additional data points from this study give a much better constrained value (Table 5). Together with the estimate of the monoclinic pyrrhotite fraction based on M_s measurements (Table 1) it emerges that monoclinic pyrrhotite has a value for its magnetocrystalline anisotropy constant that is ~ 15 per cent lower than previously known. However, some caution is appropriate: the total number of data points still is not very large and stoichiometric information on the previously reported data is lacking. In addition to the estimate of the monoclinic pyrrhotite fraction we provide the information obtained from the analysis of the AMS tensor, which also gives a first-order approximation about the purity of the very crystal utilized in the torque data acquisition. In this context, AMS measurements can be used as indicator of the presence of monoclinic pyrrhotite single crystals.

Thermomagnetic analysis and high-field torque magnetometry was done on different crystal fragments of the same sample. Thermomagnetic curves must be considered a good indicator of the composition of the samples, but as discussed above, the homogeneity of the crystal is always of concern particularly in the case pyrrhotite where intergrown superstructures occur as a rule. AMS, however, is done on the same sample and we considered it essential. We have only used the good stable low-field AMS tensors, the best approach to a single crystal. Some reported values seem to offer data on impure crystals (Sato *et al.* 1964) still yielding the same K_1 estimate, which could suggest that crystallographic purity arguments may be of lesser importance.

A mean value of K_1 : $(2.7 \pm 0.2) 10^4 \text{ Jm}^{-3}$ has been derived. The new value has a relative error of 3.5 per cent, one order of magnitude smaller than the previously reported value, which had a relative error of 47 per cent. The new value is more similar to the determination by Mikami *et al.* (1959) than that reported by Bin & Pauthenet (1963), which is the most commonly used (Dunlop & Özdemir 1997).

ACKNOWLEDGMENTS

Six of our samples have been kindly provided by T. Senior from the Utrecht University collection and the other five by J.-P. Lorand of the Museum National D'Histoire Naturelle, Paris. M.L. Osete is thanked for allowing the access to her lab facilities. The manuscript has benefited from the comments of GJI reviewers Adrian Muxworthy and Pierre Rochette, which were appreciated. This work has been supported by a Marie Curie Fellowship to FMH (project number MEIF-CT-2003-502133).

REFERENCES

- Arnold, R.G., 1967. Range in composition and structure of 82 natural terrestrial pyrrhotites, *Can. Min.*, **9**, 31–50.
- Bennett, C.E.G. & Graham, J., 1980. New observations on natural pyrrhotites. Part III. Thermomagnetic experiments, *Am. Mineral.*, **65**, 800–807.
- Bennett, C.E.G. & Graham, J., 1981. New observations on natural pyrrhotites: magnetic transition in hexagonal pyrrhotite, *Am. Mineral.*, **66**, 1254–1257.
- Bertaut, E.F., 1953. Contribution à l'étude des structure lacunaires: la pyrrhotine, *Acta Cryst.*, **6**, 557–561.
- Bin, M. & Pauthenet, R., 1963. Magnetic anisotropy in pyrrhotite, *J. appl. Phys.*, **34**, 1161–1162.
- Bottoni, G., 1995. Rotational hysteresis and magnetic anisotropy of particle for magnetic recording, *J. Magnet. Magnet. Mater.*, **140**, 2207–2208.
- Bottoni, G., Candolfo, D., Cecchetti, A. & Masoli, F., 1999. Analysis of the magnetization switching using the rotational hysteresis integral, *J. Magnet. Magnet. Mater.*, **193**, 329–331.
- Bozorth, R.M., 1951. *Ferromagnetism*. Van Nostrand, Princeton, 968 pp.
- Clark, D.A., 1984. Hysteresis properties of sized dispersed monoclinic pyrrhotite grains, *Geophys. Res. Lett.*, **11**, 173–176.
- Collinson, D.W. & Creer, K.M., 1960. Measurements in palaeomagnetism, in *Methods and Techniques in Geophysics*, pp. 168–210, eds S.K. Runcorn. Interscience Publishers, Inc., New York.
- Day, R., O'Reilly, W. & Banerjee, S.K., 1970. Rotational hysteresis study of oxidized basalts, *J. geophys. Res.*, **75**, 375–386.
- de Wall, H. & Nano, L., 2004. The use of field dependence of magnetic susceptibility for monitoring variations in titanomagnetite composition—a case study on basanites from the Vogelsberg 1996 Drillhole, Germany, *Studia Geophysica et Geodaetica*, **48**, 767–776.
- de Wall, H. & Worm, H.-U., 1993. Field dependence of magnetic anisotropy in pyrrhotite: effects of texture and grain shape, *Phys. Earth planet. Inter.*, **76**, 137–149.
- Dekkers, M.J., 1988. Magnetic properties of natural pyrrhotite. Part I: behaviour of initial susceptibility and saturation-magnetization-related rock-magnetic parameters in a grain-size dependent framework, *Phys. Earth planet. Inter.*, **52**, 376–393.
- Dunlop, D.J. & Özdemir, Ö., 1997. *Rock Magnetism: Fundamentals and Frontiers*, Cambridge Studies in Magnetism. Cambridge University Press, Cambridge, 573 pp.
- Egli, R., 2003. Analysis of the field dependence of remanent magnetization curves, *J. geophys. Res.*, **108**, art. no.-2081.
- Evans, M.E. & Heller, F., 2003. *Environmental Magnetism: Principles and Applications of Enviromagnetics*, International Geophysics Series, 86. Academic Press, London, 299 pp.
- Fabian, K., 2006. Approach to saturation analysis of hysteresis measurements in rock magnetism and evidence for stress dominated magnetic anisotropy in young mid-ocean ridge basalt, *Phys. Earth planet. Inter.*, **154**, 299–307.
- Geiss, C.E. & Zanner, C.W., 2006. How abundant is pedogenic magnetite? Abundance and grain size estimates for loessic soils based on rock magnetic analyses, *J. geophys. Res.*, **111**.
- Heslop, D., McIntosh, G. & Dekkers, M.J., 2004. Using time- and temperature-dependent Preisach models to investigate the limitations of modelling isothermal remanent magnetization acquisition curves with cumulative log Gaussian functions, *Geophys. J. Int.*, **157**, 55–63.
- Hirone, T., Adachi, K., Yamada, M., Chiba, S. & Tazawa, S., 1962. The magnetic anisotropy of pyrrhotite and iron selenide, *J. Phys. Soc. Jpn.*, **17**, 257–260.
- Horng, C.S. & Roberts, A.P., 2006. Authigenic or detrital origin of pyrrhotite in sediments?: resolving a paleomagnetic conundrum, *Earth planet. Sci. Lett.*, **241**, 750–762.
- Hrouda, F., 2002. Low-field variation of magnetic susceptibility and its effect on the anisotropy of magnetic susceptibility of rocks, *Geophys. J. Int.*, **150**, 715–723.
- Hrouda, F., Chlupacova, M. & Mrazova, S., 2006a. Low-field variation of magnetic susceptibility as a tool for magnetic mineralogy of rocks, *Phys. Earth planet. Inter.*, **154**, 323–336.
- Hrouda, F., Chlupacova, M. & Pokorny, J., 2006b. Low-field variation of magnetic susceptibility measured by the KLY-4S Kappabridge and KLY-4A magnetic susceptibility meter: accuracy and interpretational programme, *Stud. Geophys. Geodyn.*, **50**, 283–298.
- Jackson, M.J., Moskowitz, B.M., Rosenbaum, J. & Kissel, C., 1998. Field-dependence of AC susceptibility in titanomagnetites, *Earth planet. Sci. Lett.*, **157**, 129–139.
- Jelinek, V., 1973. Precision A.C. bridge set for measuring magnetic susceptibility of rocks and its anisotropy, *Stud. Geophys. Geodyn.*, **17**, 36–48.
- Jelinek, V., 1978a. Statistical processing of magnetic susceptibility measured on groups of specimens, *Stud. Geophys. Geodyn.*, **22**, 50–62.
- Jelinek, V., 1978b. Statistical processing of magnetic susceptibility measured on groups of specimens, *Stud. Geophys. Geodyn.*, **22**, 50–62.
- Keller, R. & Schmidbauer, E., 1999. Magnetic hysteresis properties and rotational hysteresis losses of synthetic stress-controlled titanomagnetite (Fe_{2.4}Ti_{0.6}O₄) particles – II. Rotational hysteresis losses, *Geophys. J. Int.*, **138**, 334–342.
- Kissin, S.A. & Scott, S.D., 1982. Phase relations involving pyrrhotite below 350 °C, *Econ. Geol.*, **77**, 1739–1754.
- Kruiver, P.P., Dekkers, M.J. & Heslop, D., 2001. Quantification of magnetic coercivity components by the analysis of acquisition curves of isothermal remanent magnetisation, *Earth planet. Sci. Lett.*, **189**, 269–276.
- Launeau, P. & Robin, P.-Y.F., 2005. Determination of fabric and strain ellipsoids from measured sectional ellipses—implementation and applications, *J. Struct. Geol.*, **27**, 2223–2233.
- Lindsley, D.H., Andreasen, G.E. & Balsley, J.R., 1966. Magnetic properties of rocks and minerals, in *Handbook of Physical Constants*, pp. 543–552, eds S.P. Clark. Geological Society of America, New York.
- Martin-Hernandez, F. & Hirt, A.M., 2004. A method for the separation of paramagnetic, ferrimagnetic and hematite magnetic subfabrics using high-field torque magnetometer, *Geophys. J. Int.*, **157**, 117–127.
- Martin-Hernandez, F., Bominaar-Silkens, I.M., Dekkers, M.J. & Maan, J.K., 2006. High-field cantilever magnetometry as a tool for the determination of the magnetocrystalline anisotropy of single crystals, *Tectonophysics*, **418**, 21–30.
- Mikami, I., Hirone, T., Watanabe, H., Maeda, S., Adachi, K. & Yamada, M., 1959. On the Magnetic Anisotropy of a Pyrrhotite Crystal, *J. Phys. Soc. Jpn.*, **14**, 1568–1572.
- Morimoto, N., Nakazawa, H., Nishiguchi, K. & Tokonami, M., 1970. Pyrrhotites: schistometric compounds with composition Fe_{n-1}S_n (n GE 8), *Science*, **168**, 964–966.
- Moskowitz, B.M., 1981. Methods for estimating Curie temperatures of titanomaghemites from experimental J_s-T data, *Earth planet. Sci. Lett.*, **53**, 84–88.
- Mullender, T.A.T., van Velzen, A.J. & Dekkers, M.J., 1993. Continuous drift correction and separate identification of ferrimagnetic and paramagnetic contributions in thermomagnetic runs, *Geophys. J. Int.*, **114**, 663–672.
- Muxworthy, A.R., 2002. Magnetic hysteresis and rotational hysteresis properties of hydrothermally grown multidomain magnetite, *Geophys. J. Int.*, **149**, 805–814.
- Muxworthy, A.R., Schmidbauer, E. & Petersen, N., 2002. Magnetic properties and Mossbauer spectra of urban atmospheric particulate matter: a case study from Munich, Germany, *Geophys. J. Int.*, **150**, 558–570.

- Muxworthy, A.R., King, J.G. & Heslop, D., 2005. Assessing the ability of first-order reversal curve (FORC) diagrams to unravel complex magnetic signals, *J. geophys. Res.*, **110**, doi:10.1029/2004JB003195.
- Naldrett, A.J. & Kullerud, G., 1967. A study of the Strathcona mine and its bearing on the origin of the nickel-copper ores of the Sudbury district, Ontario, *J. Petrol.*, **8**, 453–534.
- Neel, L., 1942. Theory of Rayleigh's law of magnetization, *Cahier. Phys.*, **12**, 1–20.
- O'Reilly, W., Hoffmann, V., Chouker, A.C., Soffel, H.C. & Menyeh, A., 2000. Magnetic properties of synthetic analogues of pyrrhotite ore in the grain size range 1–24 μm , *Geophys. J. Int.*, **142**, 669–683.
- Owens, W.H., 1981. A simple model for non-vanishing rotational hysteresis in haematite, *Phys. Earth planet. Inter.*, **27**, 106–113.
- Peters, C. & Dekkers, M.J., 2003. Selected room temperature magnetic parameters as a function of mineralogy, concentration and grain size, *Phys. Chem. Earth*, **28**, 659–667.
- Pike, C.R., Roberts, A.P. & Verosub, K.L., 1999. Characterizing interactions in fine magnetic particle systems using first order reversal curves, *J. appl. Phys.*, **85**, 6660–6667.
- Pike, C.R., Roberts, A.P., Dekkers, M.J. & Verosub, K.L., 2001. An investigation of multi-domain hysteresis mechanisms using FORC diagrams, *Phys. Earth planet. Inter.*, **126**, 11–25.
- Pokorný, J., Suza, P. & Hrouda, F., 2004. Anisotropy of magnetic susceptibility of rocks measured in variable weak magnetic fields using the KLY-4S Kappabridge, in *Magnetic Fabric: Methods and Applications*, pp. 69–76, eds, F. Martín-Hernández, C. Lüneburg, C. Aubourg & M. Jackson, Special Publications. Geological Society of London, London.
- Roberts, A.P., Cui, Y.-L. & Verosub, K.L., 1995. Wasp-waisted hysteresis loops: mineral magnetic characteristics and discrimination of components in mixed magnetic systems, *J. geophys. Res. B: Solid Earth*, **100**, 17 909–17 924.
- Roberts, A.P., Pike, C.R. & Verosub, K.L., 2000. First-order reversal curve diagrams: a new tool for characterising the magnetic properties of natural samples, *J. geophys. Res.*, **102**, 28 461–28 475.
- Robion, P. & Borradaile, G., 2001. Stress remagnetization in pyrrhotite-calcite synthetic aggregates, *Geophys. J. Int.*, **144**.
- Sato, K., Yamada, M. & Hirone, T., 1964. Magnetocrystalline anisotropy of pyrrhotite, *J. Phys. Soc. Jpn.*, **19**, 1592–1595.
- Schmidbauer, E., 1988. Magnetic rotational hysteresis study of spherical 85–160 nm Fe_3O_4 particles, *Geophys. Res. Lett.*, **15**, 522–525.
- Schmidbauer, E. & Keller, R., 1994. Magnetic properties and rotational hysteresis of a basalt with homogeneous Ti-rich titanomagnetite grains 10–20 μm in diameter, *Geophys. J. Int.*, **119**, 880–892.
- Schwarz, E.J., 1975. Magnetic properties of pyrrhotite and their use in applied geology and geophysics, *Geol. Surv. Can. Paper*, **74–59**, 24 pp.
- Schwarz, E. & Vaughan, D.J., 1972. Magnetic phase relations of pyrrhotite, *J. Geomag. Geoelectr.*, **24**, 441–458.
- Snowball, I. & Torii, M., 1999. Incidence and significance of magnetic iron sulphides in Quaternary sediments and soils, in *Quaternary Climates, Environments and Magnetism*, pp. 199–230, eds, B.A. Maher & R. Thompson. University Press, Cambridge.
- Spassov, S., Egli, R., Heller, F., Nougaliiev, D.K. & Hannam, J., 2004. Magnetic quantification of urban pollution sources in atmospheric particulate matter, *Geophys. J. Int.*, **159**, 555–564.
- Stacey, F.D., 1963. The physical theory of rock magnetism, *Adv. Phys.*, **12**, 45–133.
- Tauxe, L., Mullender, T.A.T. & Pick, T., 1996. Potbellies, wasp-waists, and superparamagnetism in magnetic hysteresis, *J. geophys. Res. B: Solid Earth*, **101**, 571–583.
- Vaughan, D.J. & Graig, J.R., 1978. *Mineral Chemistry of Metal Sulfides*, Cambridge University Press, Cambridge, 493 pp.
- Wehland, F., Stancu, A., Rochette, P., Dekkers, M.J. & Appel, E., 2005. Experimental evaluation of magnetic interaction in pyrrhotite bearing samples, *Phys. Earth planet. Inter.*, **153**, 181–190.
- Worm, H.-U., 1991. Multidomain susceptibility and anomalously strong low field dependence of induced magnetization in pyrrhotite, *Phys. Earth planet. Inter.*, **69**, 112–118.
- Worm, H.-U., Clark, D. & Dekkers, M.J., 1993. Magnetic susceptibility of pyrrhotite: grain size, field and frequency dependence, *Geophys. J. Int.*, **114**, 127–137.
- Yoshida, Y., Templeton, T.L. & Arrott, A.S., 1994. Model-calculations of rotational hysteresis for ferromagnetic particles with competing anisotropies, *J. appl. Phys.*, **75**, 5695–5697.
- Zapletal, K., 1993. Effect of intergrowths of the ferrimagnetic and antiferromagnetic phases on the rock magnetic properties of natural pyrrhotites, *Phys. Earth planet. Inter.*, **76**, 151–162.